IEEE Access
Multidisciplinary | Rapid Review | Open Access Journal

Received April 4, 2019, accepted April 17, 2019, date of publication May 15, 2019, date of current version June 21, 2019.

Digital Object Identifier 10.1109/ACCESS.2019.2917035

Buoyancy Effects on MHD Transport of Nanofluid Over a Stretching Surface With Variable Viscosity

BANDAR BIN-MOHSIN
Department of Mathematics, College of Science, King Saud University, Riyadh 11451, Saudi Arabia
e-mail: bbmohsincoll2019@gmail.com

Author thank the support of a grant from the Deanship of Scientific Research, King Saud University through Research Group RG-1437-019.

ABSTRACT In this mathematical study, the time-independent, incompressible, magneto-hydrodynamic nanofluid flow over a vertical stretching surface has been investigated. The impact of gravitational body forces along with convective boundary condition has also been a part of this study. The viscous effects of nanofluid are assumed to be temperature-dependent and in this context, the Reynolds exponential viscosity model has been employed. It is also assumed that the base fluid contains a uniform suspension of nanoparticles. The Buongiorno model comprising the thermophoresis and Brownian motion effects have been taken into account. For the sake of solution, the Runge-Kutta-Fehlberg method has been selected and the resulting outcomes have been compared with the previously published data. Moreover, the graphical plots illustrating the impact of various emerging entities on the momentum, mass, and heat transfer properties have also been provided. It has been noticed that the nanofluid viscosity parameter decelerates the fluid velocity, however, a reversed phenomenon has been achieved for the temperature and the concentration profile. Also, an augmentation in Nusselt number has been noted with the increased thermal and species Grashof numbers.

INDEX TERMS Buoyancy, convective boundary condition, thermophoresis, MHD flow, Brownian motion, Runge-Kutta-Fehlberg scheme, numerical results.

I. INTRODUCTION

In recent years, an active research work related to the performance and heat management characteristics of nanomaterials has been conducted in various fields of engineering and applied sciences. The main objective of these research work is to fulfill the demands for the compact design of energy efficient devices, which can be found in numerous fields of engineering including chemical, electrical, aerospace, biomedical, and mechanical engineering. The aim of these steps is to enhance the effective cooling properties of microsystem cooling devices. Among the variety of nanomaterials, nanofluids have gained considerable attention. Nanofluids, introduced by Choi [1], [2], has a significant impact on the thermal as well as the convective heat exchange properties as compared to the traditional host fluid like air, ethylene glycol, water, etc. The synthetic composition of nanofluids involves a variety of nano-meter sized particles including metallic (copper, silver, alumina) or non-metallic (graphene, carbon nanotubes) into the host fluid. The innovative features of nanofluids can practically be applicable in solar cell development [3], cancer treatment [4], [5], anti-bacterial structures [6], [7], and coolants in various mechanical and electrical devices [8]–[10]. In this context, Buongiorno [11] presented a comprehensive model that incorporates the variety of nanofluids and unveils the all possible thermal as well as the convective features that can hardly be found in common fluids.

The flow of boundary layer nature, due to the practical applications like manufacturing of glass fiber, production of rubber and polymer surfaces, etc., have caught the sight of worldwide scientists in the recent past decades. In this regard, a rudimentary work has been delivered by Khan *et al.* [12], where nonlinear radiation effects on MHD flow of nanofluid over a nonlinearly stretching/shrinking wedge. Later on, by incorporating the nanofluids, some tangible results were obtained by various researchers, see [13]–[17]. After the pioneering work, considerable research work has been presented by several authors. Some of these can be found in [18]–[20] and references therein.

The magneto-hydro dynamics phenomenon has found potential applications in numerous engineering and industrial processes. By employing the magnetic field effects, the fluid velocity along with the convective thermo-magnetic current

The associate editor coordinating the review of this manuscript and approving it for publication was Shuai Liu.

can be easily controlled, which then enable us to adjust the rate of flow and heat exchange processes [21]. The behavior of nanofluid, under the impact of an externally applied magnetic field, towards an elastic expanding surface, have been investigated by many scientists like Akbar *et al.* [22], [23]. Recently, several authors have investigated the flow problems of boundary layer nature along with the convective surface auxiliary condition. In this context, Aziz [24] presented a pioneering work by considering the thermal boundary layer flow together with convective auxiliary condition towards a flat stretching surface. By employing the Sakiadis as well as Blasius flows, Bataller [25] extended Aziz's work [26], by incorporating both radiative effects and convective boundary condition. Furthermore, the reader can find the most relatable studies in [27]–[30].

The objective of this study is to explore the magneto-hydrodynamic nanofluid flow over a vertical expanding surface. The impact of gravitational body forces along with convective auxiliary condition have also a part of this study. Moreover, the viscous effects of nanofluid are assumed to be temperature-dependent and in this context, the Reynolds exponential viscosity model has been considered. Shooting method accompanied by Runge-Kutta-Fehlberg scheme has been employed, for the sake of solution. Furthermore, the graphical plots along with a comprehensive discussion related to the velocity as well as temperature and concentration profiles, under the impact of several meaningful entities, have also been presented.

II. MATHEMATICAL MODEL

An incompressible, time-independent, laminar and magneto-hydrodynamic viscid flow of a nanofluid, towards a vertical expanding surface, have been under consideration, where (x, y) is chosen as a coordinate system, with the assumption that the surface is aligned with the $x-$ axis. Moreover, a cross magnetic field, with strength B_0, is applied in the transverse direction. The nanofluid, under consideration, is a homogenous dilute mixture, in which the nanomaterials are equally dispersed. The surface is supposed to be stretchable, with the linear stretching velocity $u(x) = bx$, with $b > 0$ is a constant. The temperature of the surface is due to the convective process of heating, which can be characterized by the coefficient of heat transfer h_f and the temperature of the fluid k_f. Under the aforesaid assumptions, the conservative equations for mass and momentum together with energy and nanocomposite diffusion are mathematically expressed as [23]:

$$\left(\frac{\partial u}{\partial x}+\frac{\partial v}{\partial y}\right)=0, \tag{1}$$

$$\rho\left[\left(\frac{\partial u}{\partial x}\right)u+\left(\frac{\partial u}{\partial y}\right)v\right]=-\sigma B_0^2 u+\rho g\beta_T\left(T-T_\infty\right)+g\rho\beta_C\left(C-C_\infty\right)+\frac{\partial}{\partial y}\left[\mu\left(T\right)\left(\frac{\partial u}{\partial y}\right)\right], \tag{2}$$

$$\rho c_p\left[u\frac{\partial T}{\partial x}+v\frac{\partial T}{\partial y}\right]=k\frac{\partial^2 T}{\partial y^2}+\delta\left(D_B\frac{\partial T}{\partial y}\frac{\partial C}{\partial y}+\frac{D_T}{T_\infty}\left(\frac{\partial T}{\partial y}\right)^2\right), \tag{3}$$

$$u\frac{\partial \phi}{\partial x}+v\frac{\partial \phi}{\partial y}=D_B\left(\frac{\partial^2 C}{\partial y^2}\right)+\frac{D_T}{T_\infty}\left(\frac{\partial^2 T}{\partial y^2}\right), \tag{4}$$

where, u is the velocity constituents along the $x-$ direction and v along the $y-$ direction. B_0 denote the magnetic field strength, while C and T are concentration and temperature of the nanofluids, respectively. Moreover, $\delta = (\rho c)_p / (\rho c)_f$, which indicate the ratio of effective heat capacity of nanocomposites to the heat capacity of host fluid.

The related auxiliary conditions are given as:

$$\text{for } y=0,\quad u=u_w(x)=bx,\ v=0,\quad C=C_w,\ k_f\frac{\partial T}{\partial y}=h_f\left(T-T_f\right), \tag{5}$$

$$\text{as } y\to\infty,\quad u,\ v\to 0,\ C\to C_\infty,\ T\to T_\infty. \tag{6}$$

The dimensionless variables and the similarity transformations are defined as [23]:

$$u=bx\frac{d}{d\zeta}\tilde{f}(\zeta),\quad v=-(bv)^{0.5}\tilde{f}(\zeta),\quad \zeta=\left(\frac{b}{v}\right)^{0.5}y,\quad \tilde{\phi}(\zeta)=\frac{C-C_\infty}{C_w-C_\infty},\quad \tilde{\theta}(\zeta)=\frac{T-T_\infty}{T_w-T_\infty} \tag{7}$$

The viscosity of the fluid, in Eq. (2), is temperature dependent that may vary exponentially (Reynolds exponential model for viscosity) [30]. Mathematically:

$$\mu(T)=\mu_0 e^{-H(T-T_\infty)}. \tag{8}$$

where, the strength dependency among T and $\mu(T)$ are denoted by H. μ_0 indicates the viscosity of the fluid at the reference temperature T_∞. Using the similarity transform defined in Eq. (7) and then taking the Maclaurin's expansion, we get the following expression [30]:

$$e^{-\lambda\tilde{\theta}}=1-\lambda\tilde{\theta}+O\left(\lambda^2\right). \tag{9}$$

Now, by using the similarity transforms (Eq. (7)), the following dimensionless system has been achieved,

$$\left(1-\left(\lambda\tilde{\theta}\right)\right)\frac{d^3\tilde{f}}{d\zeta^3}-\lambda\frac{d\tilde{\theta}}{d\zeta}\frac{d^2\tilde{f}}{d\zeta^2}+\tilde{f}\frac{d^2\tilde{f}}{d\zeta^2}-\left(\frac{d\tilde{f}}{d\zeta}\right)^2-M^2\frac{d\tilde{f}}{d\zeta}+Gr\tilde{\theta}+Br\tilde{\phi}=0, \tag{10}$$

$$\frac{1}{\Pr}\frac{d^2\tilde{\theta}}{d\zeta^2}+\tilde{f}\frac{d\tilde{\theta}}{d\zeta}+Nb\frac{d\tilde{\theta}}{d\zeta}\frac{d\tilde{\phi}}{d\zeta}+Nt\left(\frac{d\tilde{\theta}}{d\zeta}\right)^2=0, \tag{11}$$

$$\frac{d^2\tilde{\phi}}{d\zeta^2}+Sc\tilde{f}\frac{d\tilde{\phi}}{d\zeta}+\left(\frac{Nt}{Nb}\right)\frac{d^2\tilde{\theta}}{d\zeta^2}=0. \tag{12}$$

The transformed auxiliary conditions are given as under:

$$\begin{aligned} At\,\zeta &= 0, \quad \tilde{f}(\zeta) = 0,\ \tilde{\phi}(\zeta) = 1, \\ \frac{d}{d\zeta}\tilde{\theta}(\zeta) &= -Bi\left(1 - \tilde{\theta}(\zeta)\right), \\ \frac{d}{d\zeta}\tilde{f}(\zeta) &= 1, \end{aligned} \tag{13}$$

$$\begin{aligned} As\,\zeta &\to \infty, \quad \tilde{\theta}(\zeta) = \tilde{\phi}(\zeta) = 0, \\ \frac{d}{d\zeta}\tilde{f}(\zeta) &= 0. \end{aligned} \tag{14}$$

The dimensionless numbers, arising in the set of Eqs. (10)-(14), are defined as:

$$\begin{aligned} M^2 &= \frac{B_0^2\sigma}{\rho b}, \quad \lambda = H\left(T_w - T_\infty\right), \\ \nu &= \frac{\mu_0}{\rho}, \quad Pr = \frac{\nu}{\alpha},\ R_{ex} = \frac{u_w(x)\,x}{\nu}, \\ G_T &= \frac{\rho g x^3 \beta_T \left(T_w - T_\infty\right)}{\nu^2}, \\ Nt &= \frac{\rho\tau D_T \left(T_w - T_\infty\right)}{\mu_0 T_\infty}, \\ Nb &= \frac{\rho\tau D_B \left(\phi_w - \phi_\infty\right)}{\mu_0}, \\ B_T &= \frac{\rho g x^3 \beta_C \left(C_w - C_\infty\right)}{\nu^2}, \quad Br = \frac{B_T}{R_{ex}^2}, \\ Gr &= \frac{G_T}{R_{ex}^2}, \quad Sc = PrLe. \end{aligned} \tag{15}$$

where, M is the magnetic Hartmann number, λ is the variable viscosity parameter, Pr is the Prandtl number, R_{ex} is the local Reynolds number. Moreover, the local thermal Grashof number is symbolized by G_T, while, Nt is the thermophoresis parameter. B_T is the local concentration Grashof number, Nb is the Brownian motion parameter, Sc is the Schmidt number, Br and Gr are concentration and thermal Grashof numbers.

The physical quantities like the coefficient of skin friction and the local rate of heat transfer (Nusselt number) along with local rate of mass transfer (Sherwood number) are characterized as:

$$\begin{aligned} C_f &= \frac{1}{\rho}\frac{\tau_w}{u_w^2}, \\ Nu_x &= -\frac{xq_w}{k(T_w - T_\infty)}, \\ Sh_x &= -\frac{xq_m}{D(C_w - C_\infty)}, \end{aligned} \tag{16}$$

where,

$$\begin{aligned} \tau_w &= \mu(T)\frac{\partial u}{\partial y}, \\ q_w &= -k\frac{\partial T}{\partial y}, \\ q_m &= -D\frac{\partial C}{\partial y}. \end{aligned} \tag{17}$$

Therefore, the dimensionless forms for the coefficient of skin friction, local heat flux rate, and Sherwood number are given below:

$$\begin{aligned} (Re_x)^{\frac{1}{2}} C_f &= \left(1 - \lambda\tilde{\theta}(0)\right)\frac{d^2}{d\zeta^2}\tilde{f}(0), \\ (Re_x)^{\frac{1}{2}} Nu_x &= -\frac{d}{d\zeta}\tilde{\theta}(0), \\ (Re_x)^{-\frac{1}{2}} Sh_x &= -\frac{d}{d\zeta}\tilde{\phi}(0). \end{aligned} \tag{18}$$

III. SOLUTION PROCEDURE

An efficient numerical scheme, the Runge-Kutta-Fehlberg technique has been employed to solve the system of nonlinear ordinary differential equations (Eqs. (10)-(12)). The given boundary value problem (10)-(12) can be transformed into an initial value problem, by means of Shooting algorithm. Moreover, ζ_{max} have been selected in such a way that the convergent solution exists for different values of emerging entities. The convergence criteria have been set up to the fifth decimal place.

IV. RESULTS AND DISCUSSION

This segment is prepared to investigate the performance of dimensionless axial velocity component $\tilde{f}'(\zeta)$ and temperature distribution $\tilde{\theta}(\zeta)$ together with the concentration $\tilde{\phi}(\zeta)$ profile, under the impact of numerous emerging entities like viscosity parameter λ, Hartmann number M, thermal Grashof number Gr, thermophoresis parameter Nt, concentration Grashof number Br, Brownian motion parameter Nb, Biot number Bi and Schmidt number Sc. Moreover, the acquired results for local Nusselt number as well as the coefficient of skin friction have been compared with the existing results of [23] and presented in the form of tables.

Figures 2-4 have been designed to see the impact of viscosity parameter λ, species (concentration) Grashof number Br, Hartman number M, and thermal Grashof number Gr, on the axial component of velocity. In all the cases, a maximum velocity profile have been attained near the wall ($\zeta = 0$) and gradually exhibit a nonlinear decaying behavior. Moreover, in all the upcoming figures, the magnitude of velocity profiles have been provided for two distinct viscosity parameter (λ) values: (i) constant viscosity parameter i.e., $\lambda = 0$ (displayed as solid black lines) and (ii). exponentially increasing viscosity parameter i.e., $\lambda = 0.5$ (displayed as dashed black lines). From Figure 2, it has been observed that the velocity exhibit a diminishing behavior with the growing values of the viscosity parameter. The reason behind is the enhancement in the viscous effects with larger viscosity, which consequently decelerates the fluid flow. Further, an enhancement has been perceived in the thickness of the momentum boundary layer. Similarly, one can observe a retardation in the velocity behavior with the rising effects of the magnetic field (see Figure 2). This is due to the Lorentz forces, which act as a resistive forces and consequently opposes the fluid movement. Thus, the transversal imposition of the magnetic field successfully

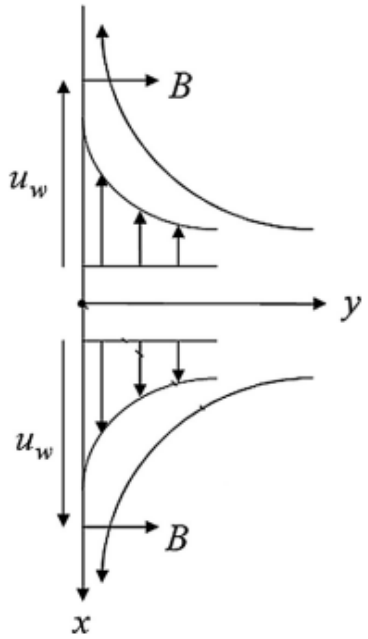

FIGURE 1. Geometrical analysis of the current flow situation.

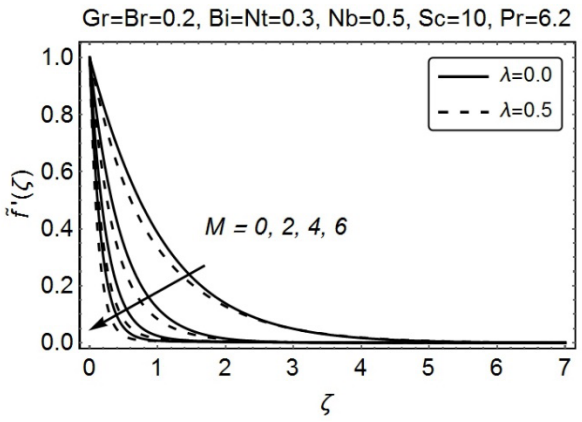

FIGURE 2. Axial velocity $\tilde{f}'(\zeta)$ behavior as *M* and λ varys.

control the fluid flow. In Figure 3, one can noticed an augmentation in the velocity profile with the growing species (concentration) Grashof number. However, the thickness of the momentum boundary layer has been declined. For $Br = 0$, the buoyancy forces related to nanoparticles species in Eq. (10) diminishes i.e. $\phi Br \rightarrow 0$. However, the non-zero values of Br depicts an overshoot in the velocity profile and this has been recorded near the stretching wall. Figure 4 demonstrates the patterns of axial velocity constituents, under the impact of thermal Grashof number Gr. The thermal buoyancy force, appearing in Eq. (10), has been vanishes, when $Gr = 0$. However, a progressive increment in the thermal buoyancy force has been noticed for $Gr = 1, 3, 5$. Moreover, for $Gr = 5$, an overshoot in the velocity profile has been observed nearby the wall, which cannot be recorded for the lesser thermal Grashof numbers. This, in turn, develops the

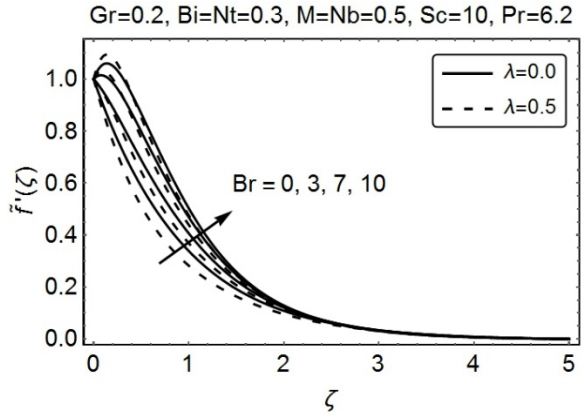

FIGURE 3. Axial velocity $\tilde{f}'(\zeta)$ behavior as *Br* and λ varys.

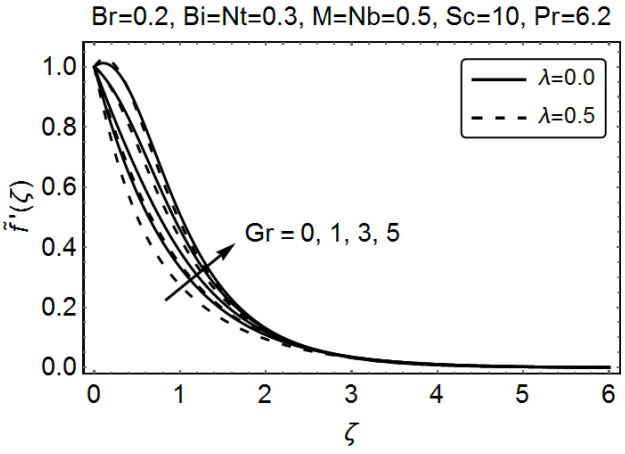

FIGURE 4. Axial velocity $\tilde{f}'(\zeta)$ behavior as *Gr* and λ varys.

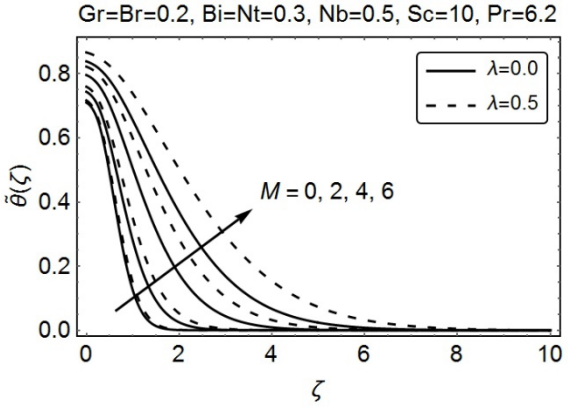

FIGURE 5. Temperature $\tilde{\theta}(\zeta)$ behavior as *M* and λ varys.

momentum inside the boundary layer and thus, leads to an increment in the fluid velocity. Furthermore, from both the figures (3 and 4), the increment in the viscous parameter opposes the fluid motion and therefore decreases the fluid velocity and enhances the thickness of momentum layer.

Figures 5-9 reveals the temperature $\tilde{\theta}(\zeta)$ patterns for varying values of viscosity parameter (λ), Hartman number (M), thermal Grashof number (Gr), concentration

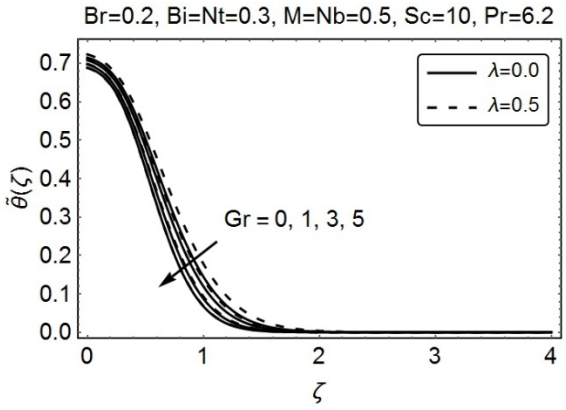

FIGURE 6. Temperature $\tilde{\theta}(\zeta)$ behavior as *Gr* and λ varys.

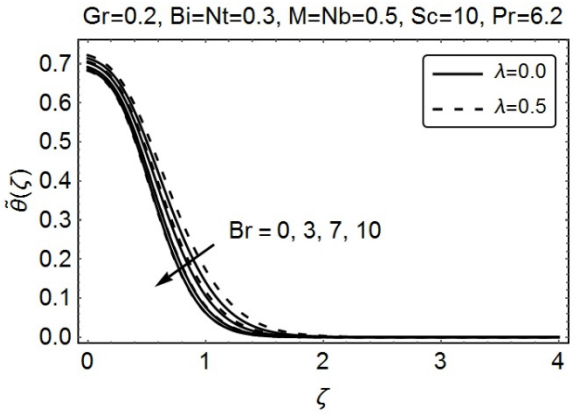

FIGURE 7. Temperature $\tilde{\theta}(\zeta)$ behavior as *Br* and λ varys.

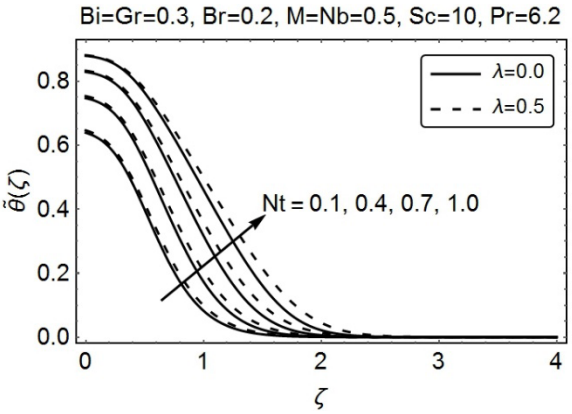

FIGURE 8. Temperature $\tilde{\theta}(\zeta)$ behavior as *Nt* and λ varys.

Grashof number (Br), thermophoresis parameter (Nt) and Biot number (Bi). For distinct values of λ (viscosity parameter): (i) $\lambda = 0$, i.e., constant viscosity parameter and (ii). $\lambda = 0.5$, i.e., exponentially increasing viscosity, the temperature depicts a different behavior as compared to velocity profile, i.e., the temperature rises with the growing viscosity parameter. Moreover, the thickness of the thermal boundary layer also increases. The impact of the Hartmann number on

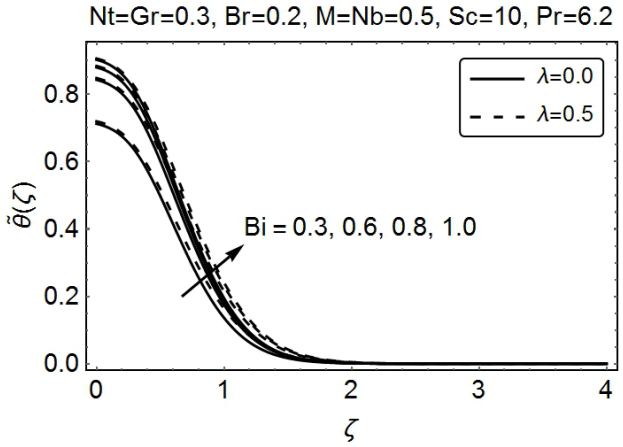

FIGURE 9. Temperature $\tilde{\theta}(\zeta)$ behavior as *Bi* and λ varys.

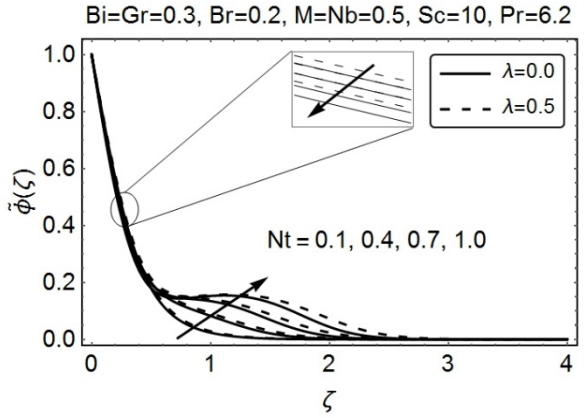

FIGURE 10. Concentration $\tilde{\phi}(\zeta)$ behavior as λ and *Nt* varys.

the temperature distribution, has been illustrated in Figure 5. The temperature elevates as the Hartmann number increases. Since the growing magnetic field enhances the friction effects within the boundary layer regime, which consequently heat up the fluid and therefore, the temperature of the fluid rises. Behavior of temperature, under the impact of thermal and species Grashof numbers, are portrayed in Figures 6 and 7, respectively. The temperature exhibit a decreasing behavior with the growing thermal Grashof number (Gr) and species Grashof number (Br). The reason behind is the decrement in the thermal diffusive process (within the boundary layer regime) with the growing values of thermal as well as the concentration buoyancy forces. The thickness of the thermal boundary layer decreases with the increasing values of both Grashof numbers. In Figure 8, the increment in the thermophoresis parameter (Nt) display a remarkable enhancement in the temperature distribution and this has been recorded throughout the boundary layer. The thermophoretic force, under the steady temperature gradient, produced by the Brownian motion of the particle. The molecules from the hotter region of the boundary layer, migrates towards the cooler area and as a result, the temperature

TABLE 1. Numerical outcomes of coefficient of skin friction, local Nusselt number, and Sherwood number, by assuming $Bi = 0.2, Sc = 10, Nt = 0.2, Nb = 0.5$ and $Pr = 6.2$.

Br	Gr	λ	$M = 0$		
			$-C_f$	Nu	Sh
0.0	0.5	0.0	0.8826	0.08681	2.3980
		0.2	0.8385	0.0864	2.3836
		0.4	0.7895	0.0859	2.3664
	1.0	0.0	0.7696	0.0874	2.4200
		0.2	0.7280	0.0871	2.4081
		0.4	0.6819	0.0867	2.3940
0.5	0.5	0.0	0.77303	0.0873	2.4144
		0.2	0.73079	0.0869	2.4018
		0.4	0.6839	0.0865	2.3870
	1.0	0.0	0.6626	0.0878	2.4353
		0.2	0.62291	0.0875	2.4249
		0.4	0.5792	0.0872	2.4129

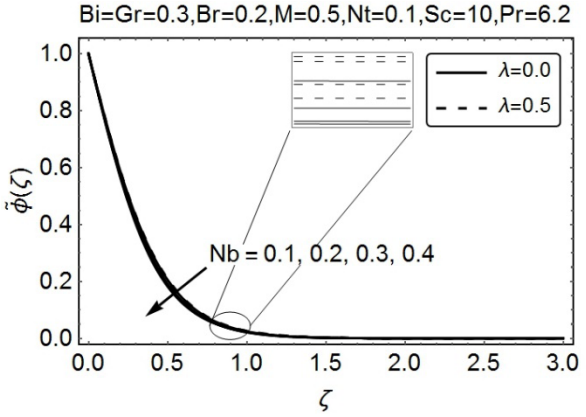

FIGURE 11. Concentration $\tilde{\phi}(\zeta)$ behavior as λ and Nb varys.

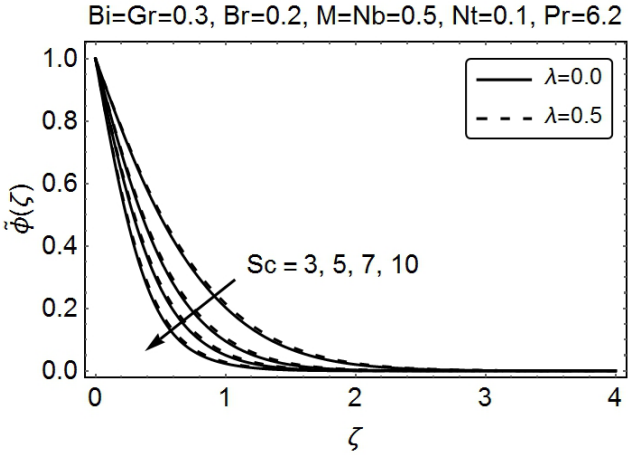

FIGURE 12. Concentration $\tilde{\phi}(\zeta)$ behavior as λ and Sc varys.

of the fluid elevates. The influence of varying values of Biot number (Bi) on the temperature distribution, has been displayed in Figure 9. The temperature exhibits an augmentation with the growing values of Biot number, which is caused by the higher fluid temperature. Moreover, from all the figures (6-9), an upsurge in temperature has been witnessed with the growing values of viscosity parameter λ.

Figures 10-12 have been sketched to see the influence of thermophoresis parameter (Nt), the Schmidt number (Sc), viscosity parameter (λ), and the Brownian motion parameter (Nb) on the dimensionless concentration profiles. For distinct values of λ (viscosity parameter): (i) $\lambda = 0$ i.e., constant viscosity parameter and (ii). $\lambda = 0.5$, i.e., exponentially increasing viscosity, the concentration profile depicts a rising behavior. The variation in concentration profile, due to varying thermophoresis parameter, have been displayed in Figure 10. With the growing thermophoresis parameter, the concentration profile depicts a strong diminishing behavior at and nearby the wall, however, far away from the stretching surface, the concentration profile displays a certain rising behavior. On the other hand, the impact of Brownian motion parameter (Nb) behaves quite differently as compared to thermophoresis parameter (Nt) (see Figure 11). The magnitude of the concentration profile depicts a declining behavior with the rising values of Nb. Physically, the larger values of Nb is due to the smaller size of the nanocomposites. This results in, an enhancement in the macro-convection and thermal conductive processes along with the diffusion process of nanoparticles species, which seems to be dominant in the region beyond the stretching wall. Thus, the rising values of Nt augments the concentration profile along with the thickness of the concentration boundary layer, however, a reversed behavior has been noticed against the rising values of Nb. Figure 12 elaborates the deviation in the $\tilde{\phi}(\zeta)$ for varying values of Sc (Schmidt number). The concentration profile reveal a decreasing behavior with growing Schmidt number. Physically, this is due to the growing rate of viscous diffusion

TABLE 2. Numerical outcomes of coefficient of skin friction, local Nusselt number, and Sherwood number, by assuming $Bi = 0.2$, $Sc = 10$, $Nt = 0.2$, $Nb = 0.5$ and $Pr = 6.2$.

Br	Gr	λ	$M = 1$		
			$-C_f$	Nu	Sh
0.0	0.5	0.0	1.2980	0.08393	2.2981
		0.2	1.2290	0.08329	2.2767
		0.4	1.1519	0.08254	2.2511
	1.0	0.0	1.1864	0.08465	2.3229
		0.2	1.1204	0.08412	2.3047
		0.4	1.0469	0.08349	2.2831
0.5	0.5	0.0	1.1898	0.08444	2.3163
		0.2	1.1229	0.08388	2.2972
		0.4	1.0486	0.08321	2.2745
	1.0	0.0	1.0807	0.0851	2.3398
		0.2	1.0169	0.0846	2.3235
		0.4	0.9464	0.0841	2.3044

TABLE 3. Numerical assessment of the outcomes of coefficient of skin friction with the published data [23], for $Bi = 0$, $Sc = 10$, $Nt = Nb = 0.5$ and $Pr = 3.97$.

Br	Gr	λ	$M = 0$		$M = 1$	
			NFD [25]	RKF	NFD [25]	RKF
0.0	0.5	0.0	0.80275	0.80274	1.22388	1.22381
		0.2	0.73278	0.73275	1.17160	1.11540
		0.4	0.64996	0.64993	0.98743	0.98739
	1.0	0.0	0.61612	0.61617	1.04352	1.04349
		0.2	0.55401	0.55398	0.94387	0.94391
		0.4	0.48181	0.48167	0.82782	0.82778
0.5	0.5	0.0	0.80532	0.80523	1.22541	1.22531
		0.2	0.73572	0.73566	1.11737	1.11742
		0.4	0.65361	0.65343	0.99022	0.99018
	1.0	0.0	0.62049	0.62035	1.04675	1.04681
		0.2	0.55874	0.55867	0.94789	0.94784
		0.4	0.48717	0.48701	0.83246	0.83250

effects as compared to the rate of mass diffusion. Therefore, for the least values of Schmidt number, one can found a maximum concentration of nanocomposites. Moreover, with the rising Schmidt number, the thickness of the concentration boundary layer descends.

Tables 1 and 2 have been designed with the numerical outcomes of the coefficient of skin friction, by assuming the cases of conducting as well as non-conducting nanofluids, respectively. Moreover, the results related to rate of heat flux (Nusselt number) along with the mass flux rate (Sherwood number) has also been provided. From these tables, one can notice an augmentation in the skin friction coefficient with the growing values of viscosity parameter (λ), concentration Grashof number (Br) and thermal Grashof number (Gr), however, a quite opposite behavior has been recorded against Hartman number (M). Moreover, the local heat flux rate as well as the Sherwood number displays a rising behavior with increasing values of Br and Gr, while a decreasing attributes have been achieved with the growing values of viscosity parameter (λ) and Hartman number (M).

For the sake of comparison between the obtained results and the previously published data, Tables 3 and 4 have been provided. The procured numerical outcomes for the local rate of heat transfer together with the coefficient of skin friction have been compared with the previously existing results [23]. The results have been displayed by taking the $Bi = 0$ and

TABLE 4. Numerical assessment of the outcomes of the local Nusselt number with the published data [23], for $Bi = 0$, $Sc = 10$, $Nt = Nb = 0.5$ and $Pr = 3.97$.

Br	Gr	λ	$M = 0$		$M = 1$	
			NFD [25]	RKF	NFD [25]	RKF
0.0	0.5	0.0	0.96539	0.96537	0.88982	0.88976
		0.2	0.95049	0.95045	0.86798	0.86806
		0.4	0.93123	0.93119	0.83988	0.83997
	1.0	0.0	0.99035	0.99031	0.91831	0.91824
		0.2	0.97937	0.97934	0.90138	0.90132
		0.4	0.96564	0.96561	0.88002	0.88000
0.5	0.5	0.0	0.96877	0.96880	0.89409	0.89405
		0.2	0.95435	0.95444	0.87314	0.87311
		0.4	0.93599	0.93594	0.84612	0.84608
	1.0	0.0	0.99321	0.99313	0.92176	0.92169
		0.2	0.98257	0.98251	0.90532	0.90525
		0.4	0.96933	0.96924	0.88449	0.88454

for both $M = 0$ and $M = 1$. The numerical outcomes are in excellent agreement with the previously published data [23].

V. CONCLUSION

This article comprises the study related to the magneto-hydrodynamic nanofluid flow, towards a vertical stretching surface along with the temperature dependent viscosity and the buoyancy effects. The impact of gravitational body forces together with convective boundary condition has also a part of this study. Runge-Kutta-Fehlberg scheme has been opted to solve the subsequent nonlinear boundary value problem and the resulting outcomes have been compared with the already published results. Moreover, the graphical pictures illustrating the impact of various emerging parameters on the momentum, mass and heat transfer properties have also been provided. The following are the main findings of this research work.

- The fluid flow decelerates with the growing values of Hartmann number, while the momentum boundary layer thickness increases.
- The thickness of the momentum boundary layer reduced while increasing the species as well as the thermal Grashof numbers. However, an accelerated flow has been perceived for the same parameters.
- Temperature elevates with the growing values of thermophoresis parameter, Hartmann number, and Biot number.
- A reduction in temperature has been detected with the growing values of thermal as well as concentration Grashof number.
- The concentration profile depicts a decline with the elevation of the Brownian motion parameter and the Schmidt number.
- The increment in the thermophoresis parameter augments the concentration distribution.
- The increasing values of viscosity parameter decelerate the nanofluid velocity magnitudes, however, enhances both the concentration and temperature distributions.
- The Nusselt number drops, while the temperature distribution rises, by means of increasing the Biot number and Hartmann number.
- An augmentation in the rate of heat flux has been noted with the increased thermal and species Grashof numbers.

REFERENCES

[1] S. U. S. Choi and J. A. Eastman, "Enhancing thermal conductivity of fluids with nanoparticles," *ASME-Publications-Fed*, vol. 231, pp. 99–106, Oct. 1995.

[2] M. A. Khairul, K. Shah, E. Doroodchi, R. Azizian, and B. Moghtaderi, "Effects of surfactant on stability and thermo-physical properties of metal oxide nanofluids," *Int. J. Heat Mass Transf.*, vol. 98, pp. 778–787, Jul. 2016.

[3] S. K. Das, S. U. S. Choi, W. Yu, and T. Pradeep, *Nanofluids: Science and Technology*. New York, NY, USA: Wiley, 2008.

[4] E. E. Michaelides, *Nanofluidics: Thermodynamic and Transport Properties*. New York, NY, USA: Springer, 2014.

[5] R. N. Mehta, M. Chakraborty, and P. A. Parikh, "Nanofuels: Combustion, engine performance and emissions," *Fuel*, vol. 120, pp. 91–97, Mar. 2014.

[6] M. M. Rashidi, S. Abelman, and N. F. Mehr, "Entropy generation in steady MHD flow due to a rotating porous disk in a nanofluid," *Int. J. Heat Mass Transf.*, vol. 62, pp. 515–525, Jul. 2013.

[7] R. Ellahi, "The effects of MHD and temperature dependent viscosity on the flow of non-Newtonian nanofluid in a pipe: Analytical solutions," *Appl. Math. Model.*, vol. 37, no. 3, pp. 1451–1467, Feb. 2013.

[8] O. D. Makinde, W. A. Khan, and Z. H. Khan, "Buoyancy effects on MHD stagnation point flow and heat transfer of a nanofluid past a convectively heated stretching/shrinking sheet," *Int. J. Heat Mass Transf.*, vol. 62, pp. 526–533, Jul. 2013.

[9] M. Sheikholeslami, M. G. Bandpy, R. Ellahi, M. Hassan, and S. Soleimani, "Effects of MHD on Cu–water nanofluid flow and heat transfer by means of CVFEM," *J. Magn. Magn. Mater.*, vol. 349, pp. 188–200, Jan. 2014.

[10] A. O. Ajibade and A. M. Umar, "Effect of chemical reaction and radiation absorption on the unsteady MHD free convection Couette flow in a vertical channel filled with porous materials," *Afrika Matematika*, vol. 27, nos. 1–2, pp. 201–213, 2016.
[11] J. Buongiorno, "Convective transport in nanofluids," *J. Heat Transf.*, vol. 128, no. 3, p. 240, 2006.
[12] U. Khan, N. Ahmed, S. T. Mohyud-Din, and B. Bin-Mohsin, "Nonlinear radiation effects on MHD flow of nanofluid over a nonlinearly stretching/shrinking wedge," *Neural Comput. Appl.*, vol. 28, no. 8, pp. 2041–2050, 2017.
[13] O. A. Bég, M. Ferdows, S. Shamima, and M. N. Islam, "Numerical simulation of Marangoni magnetohydrodynamic bio-nanofluid convection from a non-isothermal surface with magnetic induction effects: A bio-nanomaterial manufacturing transport model," *J. Mech. Med. Biol.*, vol. 14, no. 3, 2014, Art. no. 1450039.
[14] G. Huminic and A. Huminic, "Heat transfer and flow characteristics of conventional fluids and nanofluids in curved tubes: A review," *Renew. Sustain. Energy Rev.*, vol. 58, pp. 1327–1347, May 2016.
[15] O. Mahian, C. Kleinstreuer, A. Kianifar, A. Z. Sahin, G. Lorenzini, and S. Wongwises, "Entropy generation minimization in nanofluid flow," *Heat Transf. Enhancement Nanofluids*, vol. 411, pp. 411–438, Mar. 2015.
[16] B. C. Sakiadis, "Boundary-layer behavior on continuous solid surfaces: I. Boundary-layer equations for two-dimensional and axisymmetric flow," *AIChE J.*, vol. 7, no. 1, pp. 26–28, Mar. 1961.
[17] P. S. Gupta and A. S. Gupta, "Heat and mass transfer on a stretching sheet with suction or blowing," *Can. J. Chem. Eng.*, vol. 55, no. 6, pp. 744–746, 1977.
[18] C. Y. Wang, "The three-dimensional flow due to a stretching flat surface," *Phys. Fluids*, vol. 27, no. 8, pp. 1915–1917, May 1984.
[19] M.-I. Char and C.-K. Chen, "Temperature field in non-Newtonian flow over a stretching plate with variable heat flux," *Int. J. Heat Mass Transf.*, vol. 31, no. 5, pp. 917–921, 1988.
[20] R. Cortell, "MHD (magneto-hydrodynamic) flow and radiative nonlinear heat transfer of a viscoelastic fluid over a stretching sheet with heat generation/absorption," *Energy*, vol. 74, pp. 896–905, Sep. 2014.
[21] M. Sheikholeslami, D. D. Ganji, M. Y. Javed, and R. Ellahi, "Effect of thermal radiation on magnetohydrodynamics nanofluid flow and heat transfer by means of two phase model," *J. Magn. Magn. Mater.*, vol. 374, pp. 36–43, Jan. 2015.
[22] N. S. Akbar, A. Ebaid, and Z. H. Khan, "Numerical analysis of magnetic field effects on Eyring-Powell fluid flow towards a stretching sheet," *J. Magn. Magn. Mater.*, vol. 382, pp. 355–358, May 2015.
[23] N. S. Akbar, D. Tripathi, Z. H. Khan, and O. A. Bég, "A numerical study of magnetohydrodynamic transport of nanofluids over a vertical stretching sheet with exponential temperature-dependent viscosity and buoyancy effects," *Chem. Phys. Lett.*, vol. 661, pp. 20–30, Sep. 2016.
[24] A. Aziz, "A similarity solution for laminar thermal boundary layer over a flat plate with a convective surface boundary condition," *Commun. Nonlinear Sci. Numer. Simul.*, vol. 14, no. 4, pp. 1064–1068, Apr. 2009.
[25] F. G. Awad, P. Sibanda, and A. A. Khidir, "Thermodiffusion effects on magneto-nanofluid flow over a stretching sheet," *Boundary Value Problems*, vol. 2013, p. 136, 2013. [Online]. Available: http://www.boundaryvalueproblems.com/content/2013/1/136
[26] N. Bachok, A. Ishak, and I. Pop, "Unsteady boundary-layer flow and heat transfer of a nanofluid over a permeable stretching/shrinking sheet," *Int. J. Heat Mass Transf.*, vol. 55, nos. 7–8, pp. 2102–2109, Mar. 2012.
[27] R. C. Bataller, "Radiation effects for the Blasius and Sakiadis flows with a convective surface boundary condition," *Appl. Math. Comput.*, vol. 206, no. 2, pp. 832–840, Dec. 2008.
[28] O. D. Makinde and A. Aziz, "MHD mixed convection from a vertical plate embedded in a porous medium with a convective boundary condition," *Int. J. Thermal Sci.*, vol. 49, no. 9, pp. 1813–1820, Sep. 2010.
[29] A. Pantokratoras, "Buoyancy effects on thermal boundary layer over a vertical plate with a convective surface boundary condition: New results," *Meccanica*, vol. 50, no. 7, pp. 1909–1914, Jul. 2015.
[30] A. B. Disu and M. S. Dada, "Reynold's model viscosity on radiative MHD flow in a porous medium between two vertical wavy walls," *J. Taibah Univ. Sci.*, vol. 11, no. 4, pp. 548–565, 2015.

BANDAR BIN-MOHSIN received the Ph.D. degree in applied mathematics from the University of Leeds, Leeds, U.K., in 2013. He is currently an Associate Professor with the Mathematics Department, King Saud University, Saudi Arabia. He has published many papers in several high quality international journals of mathematics and engineering sciences. His research interests include numerical analysis, inverse problems, PDEs, optimization, and numerical computational methods.